

# Active Trans-Plasma Membrane Water Cycling in Yeast Is Revealed by NMR

Yajie Zhang, Marie Poirier-Quinot, Charles S. Springer Jr, James Balschi

► **To cite this version:**

Yajie Zhang, Marie Poirier-Quinot, Charles S. Springer Jr, James Balschi. Active Trans-Plasma Membrane Water Cycling in Yeast Is Revealed by NMR. *Biophysical Journal*, Biophysical Society, 2011, 101 (11), pp.2833-2842. 10.1016/j.bpj.2011.10.035 . hal-02270030

**HAL Id: hal-02270030**

**<https://hal.archives-ouvertes.fr/hal-02270030>**

Submitted on 23 Aug 2019

**HAL** is a multi-disciplinary open access archive for the deposit and dissemination of scientific research documents, whether they are published or not. The documents may come from teaching and research institutions in France or abroad, or from public or private research centers.

L'archive ouverte pluridisciplinaire **HAL**, est destinée au dépôt et à la diffusion de documents scientifiques de niveau recherche, publiés ou non, émanant des établissements d'enseignement et de recherche français ou étrangers, des laboratoires publics ou privés.

# Active Trans-Plasma Membrane Water Cycling in Yeast Is Revealed by NMR

Yajie Zhang, Marie Poirier-Quinot, Charles S. Springer Jr, James Balschi

► **To cite this version:**

Yajie Zhang, Marie Poirier-Quinot, Charles S. Springer Jr, James Balschi. Active Trans-Plasma Membrane Water Cycling in Yeast Is Revealed by NMR. *Biophysical Journal*, Biophysical Society, 2011, 101 (11), pp.2833-2842. 10.1016/j.bpj.2011.10.035 . hal-02270030

**HAL Id: hal-02270030**

**<https://hal.archives-ouvertes.fr/hal-02270030>**

Submitted on 23 Aug 2019

**HAL** is a multi-disciplinary open access archive for the deposit and dissemination of scientific research documents, whether they are published or not. The documents may come from teaching and research institutions in France or abroad, or from public or private research centers.

L'archive ouverte pluridisciplinaire **HAL**, est destinée au dépôt et à la diffusion de documents scientifiques de niveau recherche, publiés ou non, émanant des établissements d'enseignement et de recherche français ou étrangers, des laboratoires publics ou privés.

# Active Trans-Plasma Membrane Water Cycling in Yeast Is Revealed by NMR

Yajie Zhang,<sup>†</sup> Marie Poirier-Quinot,<sup>†</sup> Charles S. Springer, Jr.,<sup>‡</sup> and James A. Balschi<sup>†\*</sup>

<sup>†</sup>Physiological NMR Core Laboratory, Division of Cardiovascular Medicine, Department of Medicine, Brigham and Women's Hospital and Harvard Medical School, Boston, Massachusetts; and <sup>‡</sup>Advanced Imaging Research Center, Oregon Health Science University, Portland, Oregon

**ABSTRACT** Plasma membrane water transport is a crucial cellular phenomenon. Net water movement in response to an osmotic gradient changes cell volume. Steady-state exchange of water molecules, with no net flux or volume change, occurs by passive diffusion through the phospholipid bilayer and passage through membrane proteins. The hypothesis is tested that plasma membrane water exchange also correlates with ATP-driven membrane transport activity in yeast (*Saccharomyces cerevisiae*). Longitudinal <sup>1</sup>H<sub>2</sub>O NMR relaxation time constant ( $T_1$ ) values were measured in yeast suspensions containing extracellular relaxation reagent. Two-site-exchange analysis quantified the reversible exchange kinetics as the mean intracellular water lifetime ( $\tau_i$ ), where  $\tau_i^{-1}$  is the pseudo-first-order rate constant for water efflux. To modulate cellular ATP, yeast suspensions were bubbled with 95%O<sub>2</sub>/5%CO<sub>2</sub> (O<sub>2</sub>) or 95%N<sub>2</sub>/5%CO<sub>2</sub> (N<sub>2</sub>). ATP was high during O<sub>2</sub>, and  $\tau_i^{-1}$  was 3.1 s<sup>-1</sup> at 25°C. After changing to N<sub>2</sub>, ATP decreased and  $\tau_i^{-1}$  was 1.8 s<sup>-1</sup>. The principal active yeast ion transport protein is the plasma membrane H<sup>+</sup>-ATPase. Studies using the H<sup>+</sup>-ATPase inhibitor ebselen or a yeast genetic strain with reduced H<sup>+</sup>-ATPase found reduced  $\tau_i^{-1}$ , notwithstanding high ATP. Steady-state water exchange correlates with H<sup>+</sup>-ATPase activity. At volume steady state, water is cycling across the plasma membrane in response to metabolic transport activity.

## INTRODUCTION

Water transport across the plasma membrane is crucial to cell function. This is often characterized as a pseudo-first-order process, measured by the permeability coefficient ( $P$ ), an intrinsic membrane property. The osmotic coefficient ( $P_j$ ) is measured when net transmembrane water movement responds to an extra- and intracellular water chemical potential difference. Cell and tissue osmotic water fluxes and volume changes are measured using several techniques, a number of them optical (1). The proteins that mediate and the molecular mechanisms that regulate water transport are of great interest. A second-order process, steady-state transmembrane water molecule exchange (no net water flux or volume change), occurs even in the absence of osmotic gradients. This is characterized by the diffusional water permeability coefficient ( $P_d$ ). Steady-state exchange occurs by passive diffusion through the phospholipid bilayer and membrane proteins.

Transmembrane exchange was originally detected in cell suspensions using isotopically labeled water (2). NMR approaches have also long been used to measure reversible water-exchange kinetics in cell suspensions. Generally a paramagnetic relaxation reagent (RR<sub>e</sub>) alters the extracellular <sup>1</sup>H<sub>2</sub>O relaxation time constant ( $T_1$  or  $T_2$ ). The  $T_2$  method was introduced by Conlon and Outhred (3) and has been widely employed (4). Longitudinal magnetic resonance relaxography (MRR) distinguishes intra- (<sup>1</sup>H<sub>2</sub>O<sub>i</sub>) and

extracellular (<sup>1</sup>H<sub>2</sub>O<sub>e</sub>) signals by their  $T_1$  difference (<sup>1</sup>H<sub>2</sub>O  $T_1$  MRR/RR<sub>e</sub>) (5). These data can yield accurate intra- and extracellular mole fractions ( $p_i$  and  $p_e$ ) and the mean intracellular water molecule lifetime ( $\tau_i$ ) if equilibrium transmembrane water exchange kinetics are quantified with two-site exchange (2SX) analysis (5–7). The inverse ( $\tau_i^{-1}$ ) is the equilibrium water efflux pseudo-first-order rate constant ( $k_{ie}$ ). Mass balance gives the influx rate constant ( $k_{ei}$ ). To aid the reader, Table 1 lists the symbols and abbreviations.

At 37°C, the  $T_2$  method has measured a  $\tau_i$  value of 8.2 ms in human erythrocytes (3) and 4.5 ms in agile wallaby erythrocytes (4). The  $T_1$  approach has been applied to yeast cell suspensions (5) and rat thigh muscle in vivo (8). In densely packed yeasts,  $\tau_i$  was 672 ms and  $p_i$  was 0.35 (5). Resting rat thigh muscle data yielded  $\tau_i = 1.1$  s and the  $p_e$  was 0.11 (8). We studied isolated rat hearts during perfusion with Krebs Henseleit buffer containing RR<sub>e</sub> and found that  $\tau_i = 184$  ms (9). Interestingly, during no-flow ischemia,  $\tau_i$  increased to 280 ms. Although water exchange is thought of as a passive process, i.e., not requiring energy, the increase in  $\tau_i$  led us to speculate that, because ischemia decreases ATP concentration,  $\tau_i$  may be sensitive to cellular energetics. Because ATP is required for membrane ion pump activity and the development of the primary ion gradient, which powers secondary active symporters and antiporters, we hypothesized that transport activity may affect transmembrane water exchange or cycling.

Accordingly, the <sup>1</sup>H<sub>2</sub>O  $T_1$  MRR/RR<sub>e</sub> method was used to measure  $p_i$  and  $\tau_i$  in yeast cell suspensions maintained in different oxygenation states, which altered cellular energetics. ATP was measured by <sup>31</sup>P MRS and HPLC. We

Submitted June 28, 2011, and accepted for publication October 26, 2011.

\*Correspondence: jbaltschi@rics.bwh.harvard.edu

Marie Poirier-Quinot's present address is IR4M Imagerie en Résonance Magnétique Médicale et Multi-Modalité, UM 8081 CNRS, Univ Paris Sud, Orsay, France.

Editor: Klaus Gawrisch.

**TABLE 1** Definition of symbols and abbreviations

Abbreviations/acronyms	Definition
MRS	Magnetic resonance spectroscopy.
MRR	Magnetic resonance relaxography.
$T_1$	Longitudinal relaxation time constant.
$R_1$ ( $\equiv T_1^{-1}$ )	Longitudinal relaxation rate constant.
$T_2$	Transverse relaxation time constant.
RR <sub>e</sub>	Extracellular relaxation reagent.
GdDTPA <sup>2-</sup>	Gadolinium diethylenetriamine penta-acetate.
IR	Inversion recovery experiment for $T_1$ measurement.
$t_I$	Delay time between 180° and 90° RF pulses in IR experiment.
$R_{1L}$	Apparent $R_1$ of component with larger $T_1$ value.
$R_{1S}$	Apparent $R_1$ of component with smaller $T_1$ value.
$a_L$	Apparent population of component with larger $T_1$ value.
$a_S$	Apparent population of component with smaller $T_1$ value.
2SX	Two-site exchange analysis model used to measure equilibrium transmembrane water exchange kinetics.
$R_{10}$	Measured <sup>1</sup> H <sub>2</sub> O $R_1$ of a sample in absence of RR <sub>e</sub> .
$R_{1i}$	$R_1$ of intracellular water.
$R_{1e0}$	$R_1$ of extracellular water before RR <sub>e</sub> .
$r_{1e}$	RR <sub>e</sub> relaxivity.
$\tau_i$	Mean intracellular water molecule lifetime.
$\tau_e$	Mean extracellular water molecule lifetime.
$k_{ie}$ ( $\equiv \tau_i^{-1}$ )	Pseudo-first-order rate constant for equilibrium water efflux.
$k_{ei}$	Pseudo-first-order rate constant for equilibrium water influx.
$p_i$	Intracellular water mole fraction.
$p_e$	Extracellular water mole fraction.
$P_f$	Osmotic or hydraulic water permeability coefficient.
$P_d$	Diffusional water permeability coefficient.
$P_w$	Steady-state water permeability coefficient with active and passive components: $P_w = P_w(\text{active}) + P_w(\text{passive})$ .
$V$	Yeast cell volume.
$A$	Yeast cell surface area.
$r$	Yeast cell radius (modeled as a sphere).

found that  $\tau_i^{-1}$  ( $\equiv k_{ie}$ ) strongly correlates with cellular ATP and, more importantly, specifically with the activity of the major ion transport plasma membrane protein, a P-type H<sup>+</sup>-ATPase. These results demonstrate an active transmembrane water cycling in yeast. To our knowledge, this is the first such observation.

## MATERIALS AND METHODS

### Yeast strains and suspensions

Four *Saccharomyces cerevisiae* strains were used. Bakers yeast, Fleischmann's Fresh Active, locally purchased was washed in minimal medium twice before use. The yeast D273-10B (No. 2465) was obtained from ATCC (Manassas, VA). These yeast cells were grown in YPD medium: 1% yeast extract, 1% peptone, and 2% glucose, and harvested at midstationary phase. BY4743 yeast (ATCC: 4024376), which are heterozygous for the gene encoding P-type H<sup>+</sup>-ATPase, PMA1, (PMA1<sup>+/-</sup>), were grown in YPD to midstationary phase, harvested, and resuspended in phosphate-free media (10), shaken for 7 h, and harvested. PMA1<sup>+/-</sup> cells have reduced H<sup>+</sup>-ATPase activity (11). MR6  $\rho^+$  yeast cells (12) were grown in YPD plus adenine and harvested at midstationary phase.

Before MR experiments, yeast were washed twice with cold minimal medium (MM) and resuspended in MM to achieve a cell density of 30% wet weight/volume (w/v). MM contains 4 mM MgSO<sub>4</sub>, 13 mM KCl, 13 mM Na<sup>+</sup> (from NaOH), 50 mM MOPs; final pH = 6.6. The <sup>1</sup>H<sub>2</sub>O<sub>e</sub> RR<sub>e</sub>, Na<sub>2</sub>GdDTPA, was synthesized from Gd<sub>2</sub>O<sub>3</sub> and H<sub>2</sub>DTPA (13). An aliquot of 100 mM Na<sub>2</sub>GdDTPA stock solution was added to the MM before making up the 30% (w/v) yeast suspension. The final [RR<sub>e</sub>] was 9.3 mM.

MR measurements were done in a 20 mm O.D. MR tube fitted with two tubes that extended to near the tube bottom (7). Gas, 95% O<sub>2</sub> (O<sub>2</sub>, aerobic), or 95% N<sub>2</sub> (N<sub>2</sub>, anaerobic), each 5% CO<sub>2</sub>, flowed constantly through the tubes. Gas flow was adjusted to suspend yeast cells during MR studies, which were done at 25°C.

### Studies with ebselen (2-phenyl-1,2-benzisoselenazol-3(2H)-one)

D273-10B cells 30% (w/v) were suspended in a solution containing 4.04 mM MgSO<sub>4</sub>, 13.4 mM KCl (pH = 6.24). Suspensions were bubbled with N<sub>2</sub> for 50 min while <sup>31</sup>P MRS and <sup>1</sup>H MRS IR data sets were acquired. Then a volume of ebselen in dimethyl sulfoxide (DMSO), to yield a final extracellular concentration of 3 mM or an equal volume of DMSO, was added 2 min before the switch to O<sub>2</sub> and <sup>31</sup>P and <sup>1</sup>H IR data were acquired. Parallel studies were done to measure suspension extracellular pH (pH<sub>e</sub>) using a pH electrode and to obtain aliquots for HPLC ATP measurements.

### MR measurements and data analyses

All MR data were acquired with an Inova 9.4T spectrometer (Varian, Palo Alto, CA). Water proton, <sup>1</sup>H<sub>2</sub>O, (398.8 MHz) longitudinal relaxation rate constants ( $R_1 \equiv T_1^{-1}$ ) were measured using an IR pulse sequence:  $sw = 8000$  Hz, 2048 complex points, 64 delay increments ( $t_I$ ) between the 180° (composite) pulse and 90° RF pulse, total time 4 min. The  $t_I$  values are listed in the Supporting Material. The longitudinal magnetization ( $M_z$ ) was quantified using Bayesian analysis software, which analyzes the free induction decay (14). The midpoint of the entire IR acquisition is reported as the measurement time. Each <sup>1</sup>H<sub>2</sub>O IR  $T_1$  measurement was

followed by a  $^{31}\text{P}$  MRS acquisition (161.8 MHz) with a one-pulse sequence; free induction decays result from 208  $45^\circ$  pulses with a recycle time of 0.9 s averaged for 3.5 min. The ATP amount was measured using Bayesian analysis software.

## Relaxographic data analyses

Fully relaxed magnetization  $M_Z(\infty)$  was the average of the last two IR  $M_z(t_i)$  values and the quantity  $[(M_Z(\infty) - M_z(t_i))/2M_Z(\infty)]$  calculated. To measure the equilibrium trans-plasma membrane water exchange kinetics, we used the 2SX model for  $^1\text{H}_2\text{O}$   $T_1$  relaxation affected by water exchange (5,8). The major 2SX assumption is that water mixing within each compartment (site) is complete; i.e., fast compared with equilibrium exchange between sites. This is an excellent assumption. With a conservatively small water diffusion coefficient ( $1.5 \mu\text{m}^2/\text{s}$ ), an intracellular water molecule will translate  $10 \mu\text{m}$  in 11 ms (15). Because  $10 \mu\text{m}$  is significantly larger than the yeast cell radius, and  $\tau_i$  is hundreds of milliseconds (see below), water molecules sample the entire cell interior many times during a lifetime, meaning they are “well mixed”.

The model predicts that, under some conditions, the experimental recovery of longitudinal magnetization after inversion can be analyzed as biexponential. This is expressed in

$$M_z(t_i) = M_Z(\infty) \left[ 1 - 2[a_L \exp(-t_i R_{1L}) + a_S \exp(-t_i R_{1S})] \right], \quad (1)$$

where  $a_L$  and  $R_{1L}$  are the apparent population and relaxation rate constant, respectively, of the component with the larger  $T_1$  value, and  $a_S$  and  $R_{1S}$  are the analogous quantities for the smaller  $T_1$  value component.

The 2SX model for  $^1\text{H}_2\text{O}$   $T_1$  relaxation has seven model parameters, of which only five are independent (5). These are:  $r_{1e}$  (extracellular RR relaxivity),  $T_{1e0}^{-1}$  ( $R_{1e0}$ , for  $^1\text{H}_2\text{O}_e$  before  $\text{RR}_e$ ),  $T_{1i}^{-1}$  ( $R_{1i}$ , for  $^1\text{H}_2\text{O}_i$ ),  $\tau_i$  (mean intracellular water molecule lifetime), and  $p_i$  (intracellular water mole fraction or population). Assuming the fast exchange limit condition before  $\text{RR}_e$  arrival (a very good assumption), one could estimate a value for  $R_{1e0}$  using  $R_{10}$  as

$$R_{1e0} = \frac{(R_{10} - p_i R_{1i})}{(1 - p_i)}, \quad (2)$$

where  $R_{10}$  is the measured  $^1\text{H}_2\text{O}$   $R_1$  for the suspension before  $\text{RR}_e$ . This leaves only four parameters (16). The first two are MR quantities (dependent on  $B_0$  and temperature). The last two are physiological parameters (dependent on temperature and cell density for  $p_i$ ), which are related to the  $\tau_e$  (mean extracellular water molecule lifetime) and  $p_e$  (extracellular water mole fraction) values by equilibrium mass balance:

$$\left[ \tau_e = \tau_i \times \left( \frac{p_e}{p_i} \right); p_e = 1 - p_i \right]. \quad (3)$$

$R_{1L}$ ,  $R_{1S}$ ,  $a_S$ , and  $a_L$  can be expressed in terms of the five intrinsic system parameters,  $R_{1i}$ ,  $r_{1e}$ ,  $R_{1e0}$ ,  $\tau_i$ , and  $p_i$  in Eqs. 4–6:

$$R_{1L} = 1/2 \left[ R_{1i} + r_{1e} [\text{RR}_e] + R_{1e0} + \tau_i^{-1} + \frac{p_i}{\tau_i(1-p_i)} \right] - 1/2 \left\{ \left[ R_{1i} - r_{1e} [\text{RR}_e] - R_{1e0} + \tau_i^{-1} - \frac{p_i}{\tau_i(1-p_i)} \right]^2 + \frac{4p_i}{\tau_i^2(1-p_i)} \right\}^{1/2}, \quad (4)$$

$$R_{1S} = 1/2 \left[ R_{1i} + r_{1e} [\text{RR}_e] + R_{1e0} + \tau_i^{-1} + \frac{p_i}{\tau_i(1-p_i)} \right] + 1/2 \left\{ \left[ R_{1i} - r_{1e} [\text{RR}_e] - R_{1e0} + \tau_i^{-1} - \frac{p_i}{\tau_i(1-p_i)} \right]^2 + \frac{4p_i}{\tau_i^2(1-p_i)} \right\}^{1/2}, \quad (5)$$

$$\frac{a_S}{a_S + a_L} = 1/2 - 1/2 \times \left[ \frac{(R_{1i} - r_{1e} [\text{RR}_e] - R_{1e0})(1 - 2p_i) + \tau_i^{-1} + \frac{p_i}{\tau_i(1-p_i)}}{\left\{ \left[ R_{1i} - r_{1e} [\text{RR}_e] - R_{1e0} + \tau_i^{-1} - \frac{p_i}{\tau_i(1-p_i)} \right]^2 + \frac{4p_i}{\tau_i^2(1-p_i)} \right\}^{1/2}} \right]. \quad (6)$$

A method we term “2SX fitting” was used to extract exchange parameters from the MRR data by rearranging Eq. 1 as Eq. 7. Equations 4–6 are substituted into the right-hand side,

$$\left[ \frac{(M_Z(\infty) - M_z(t_i))}{2M_Z(\infty)} \right] = a_L \exp(-t_i R_{1L}) + a_S \exp(-t_i R_{1S}), \quad (7)$$

and  $\tau_i$ ,  $p_i$ , and  $r_{1e}$  (with fixed  $R_{1i}$  and  $R_{1e0}$ ) are adjusted to match the IR time-course,  $[(M_Z(\infty) - M_z(t_i))/2M_Z(\infty)]$ , observed at a single  $[\text{RR}_e]$  value. The value for  $R_{1i}$  was determined at  $25^\circ\text{C}$  in cell-free MM to be  $0.48 \text{ s}^{-1}$  with  $\text{O}_2$ , and  $0.42 \text{ s}^{-1}$  with  $\text{N}_2$  bubbling. The  $R_{10}$  of an  $\text{RR}_e$ -free 30% w/v yeast suspension bubbled with  $\text{O}_2$  is  $0.48 \text{ s}^{-1}$ , and bubbled with  $\text{N}_2$  is  $0.42 \text{ s}^{-1}$ . Changing the  $R_{1i}$  value, which was fixed in Eqs. 4–6 between 0.78 and  $0.42 \text{ s}^{-1}$ , does not change the resulting fitted  $t_i$  or  $p_i$  values; the fitted  $r_{1e}$  value changes  $< 1\%$ .  $R_{1i} > 0.83 \text{ s}^{-1}$  does not produce satisfactory fittings of Eq. 7 to data. Although  $R_{1e0}$  is surely smaller than  $R_{1i}$ , both values were fixed at  $0.48 \text{ s}^{-1}$ . This is consistent with Eq. 2 because realistic values for these are too small to influence the fittings. Thus, only  $\tau_i$ ,  $p_i$ , and  $r_{1e}$  parameter values were varied to optimize the fitting. The  $\text{RR}_e$  relaxivity,  $r_{1e}$ , was varied because it was anticipated to differ from the cell-free value (5). See the Results in the Supporting Material for more on  $r_{1e}$ . Water exchange parameters in Figs. 1–4 were obtained from 2SX fittings of MRR data with 9.3 mM  $\text{RR}_e$ .

Another method for extracting exchange parameters, which we term “relaxivity fitting”, adjusts Eq. 4 and/or Eq. 5 to match the  $[\text{RR}_e]$ -dependences of  $R_{1L}$  and  $R_{1S}$  quantities determined from relaxograms (5,8). Results from relaxivity fitting are shown in Fig. S4 and Table S3 in the Supporting Material, and compared with those from 2SX fitting in Table S1 and Table S2.

## Yeast suspension intra- and extracellular volumes

Suspension total intra- and extracellular water volume values were calculated using the MR measured  $p_i = 0.075 (\pm 0.007)$  ( $n = 6$ ) and  $p_e = 0.925$ . Note that, even in a yeast cell pellet, the  $p_e \sim 0.64$ . The yeast cell pellet dry-weight/wet-weight ratio was  $0.17 (\pm 0.02)$ . Thus, 3 g wet yeast equals 0.51 g dry. Final suspension total volume was 10 mL. Correcting for yeast cell mass gives water mass ( $10 - 0.51 = 9.49 \text{ g}$ )—assuming unit density, this is 9.49 mL;  $9.49 \times 0.925$  ( $p_e$ ,  $\text{O}_2$ ) = 8.78 mL  $\approx$  8.8 mL = extracellular water volume, which was used to calculate  $[\text{RR}_e]$ ; and,  $9.49 \times 0.075$  ( $p_i$ ,  $\text{O}_2$ ) = 0.71 mL = intracellular water volume.

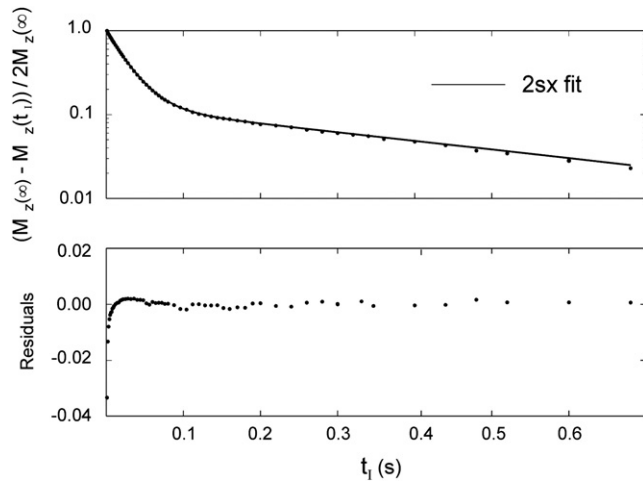


FIGURE 1  $^1\text{H}_2\text{O}$   $T_1$  MRR/RR<sub>c</sub> data and analyses. (Upper panel) 2SX fitting (solid curve) of the  $t_1$ -dependence of  $\log [(M_Z(\infty) - M_Z(t)) / 2M_Z(\infty)]$  (●) from an anaerobic ( $\text{N}_2$ ) yeast suspension with 9.3 mM RR<sub>c</sub>. Equations 4–7 were fitted to the data by adjusting  $\tau_i$ ,  $p_i$ , and  $r_{1e}$ . The values were:  $\tau_i$ , 0.536 s,  $p_i$  = 0.113, and  $r_{1e}$  = 4.07  $\text{s}^{-1} \text{mM}^{-1}$ . (Lower panel) Fitting residuals (residual = fitted curve – experiment data).

### Yeast cell volume and surface area

To estimate the  $P_w$ , we used  $P_w = \tau_i^{-1}(V/A)$ , where  $V$  and  $A$  are the individual cell volume and surface area values, respectively (5). We modeled the yeast cell as a sphere of radius  $r$ ,  $V = (4/3)\pi r^3$ ,  $A = 4\pi r^2$ ,  $V/A = r/3$ , and  $P_w = r/(3\tau_i)$ . We used a reported yeast cell intracellular water  $V$  of 42 fL (fL =  $10^{-15}$  L;

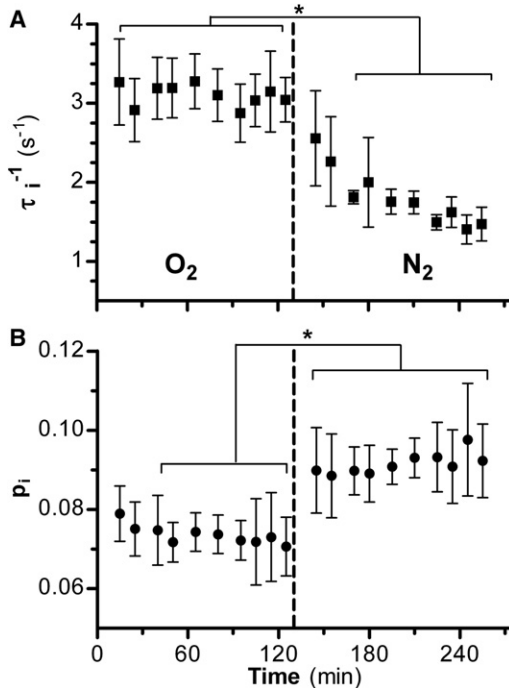


FIGURE 2 (A) Time-dependence of  $\tau_i^{-1}$  ( $\text{s}^{-1}$ ), the pseudo-first-order rate constant for equilibrium water efflux ( $k_{ie}$ ), for 30% w/v yeast suspensions during bubbling with  $\text{O}_2$  (aerobic) and after switching (dashed line) to  $\text{N}_2$  (anaerobic). (B) Time-dependence of  $p_i$ , the intracellular water mole fraction. Mean ( $\pm$  SD) of ( $n = 6$ ) D273-10B yeast cell suspensions. (Asterisk)  $p < 0.05$  repeated measures ANOVA.

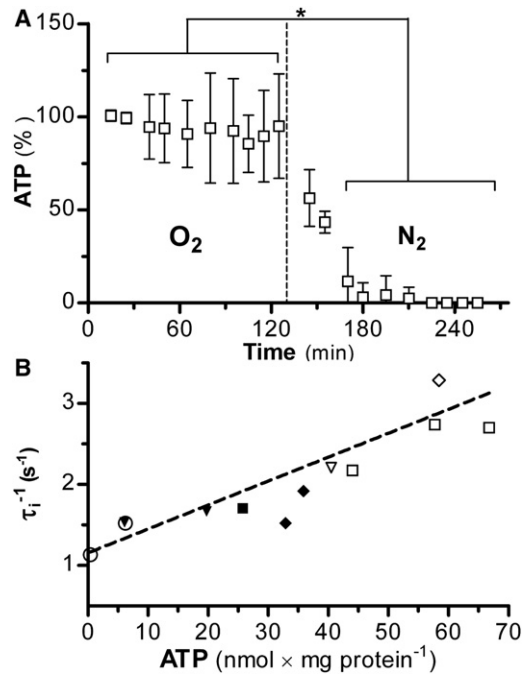


FIGURE 3 (A) Time-dependence of  $^{31}\text{P}$  MR-measured ATP content of 30% w/v suspensions of yeast bubbled with  $\text{O}_2$  (aerobic) and after switching (dashed line) to  $\text{N}_2$  (anaerobic). The  $^{31}\text{P}$  MR measures were interleaved with the  $^1\text{H}$  IR measurements used to calculate  $\tau_i^{-1}$  and  $p_i$  (Fig. 2). The first two ATP measures during  $\text{O}_2$  for each suspension were averaged and used to normalize all amounts as a percentage (%) of those measures. Mean ( $\pm$  SD) of ( $n = 6$ ) D273-10B yeast cell suspensions. (Asterisk)  $p < 0.05$  repeated measures ANOVA. (B) HPLC-measured ATP [ $\text{nmol} \times (\text{mg protein})^{-1}$ ] dependence of  $\tau_i^{-1}$  ( $\text{s}^{-1}$ ) for yeast suspensions grown and studied under various conditions. M6  $\rho+$  yeasts were grown with different adenine concentrations: 10 ( $\circ$ ), 20 ( $\blacktriangledown$ ), and, 40  $\text{mg/L}$  ( $\nabla$ ), and  $\tau_i^{-1}$  measured in aerobic ( $\square$ ) and anaerobic ( $\blacksquare$ ) conditions. D273-10B yeast were measured in aerobic ( $\diamond$ ) and anaerobic ( $\blacklozenge$ ) conditions. The best fitted line is shown: intercept,  $1.2 (\pm 0.3) \text{ s}^{-1}$ ; slope,  $0.30 (\pm 0.01) (\text{ s}^{-1} \times [\text{nmol} \times (\text{mg protein})^{-1}]^{-1})$ ;  $R^2 = 0.615$ .

1 fL =  $1 \mu\text{m}^3$ ) (17). It was assumed that this  $V$  measurement, made at low cell density, reflects the aerobic condition. The calculation returned an  $r$  value = 2.16  $\mu\text{m}$ . To adjust for the  $p_i$  increase during  $\text{N}_2$ ,  $V$  was multiplied by  $p_i(\text{N}_2)/p_i(\text{O}_2) = 1.24$ , and this returned an  $r$  of 2.32  $\mu\text{m}$ .

### HPLC analyses

ATP content was measured in perchloric acid extracts of yeast cell pellets from suspensions rapidly centrifuged at 4°C, filtered, and frozen in liquid  $\text{N}_2$ . A Macherey-Nagel nucleosil 4000-7 PEI column was employed, using a buffer A (2.5 mM Trisphosphate, pH 7.2) with 5–95% buffer B (2.5 mM Trisphosphate, 1 M KCl, pH 8.0) gradient over 20 min. The ATP retention time was 12.5 min. Protein content was determined using the Lowry method (18).

### Statistical analyses

Data are presented as the mean ( $\pm 1$  SD). Statistical computations used the software Statistica (Ver. 6.1, StatSoft, Tulsa, OK). An analysis of variance (ANOVA) compared measurements among all groups. Repeated measures ANOVA were used where appropriate. A posthoc Bonferroni test was used to compare means. Differences were declared statistically significant

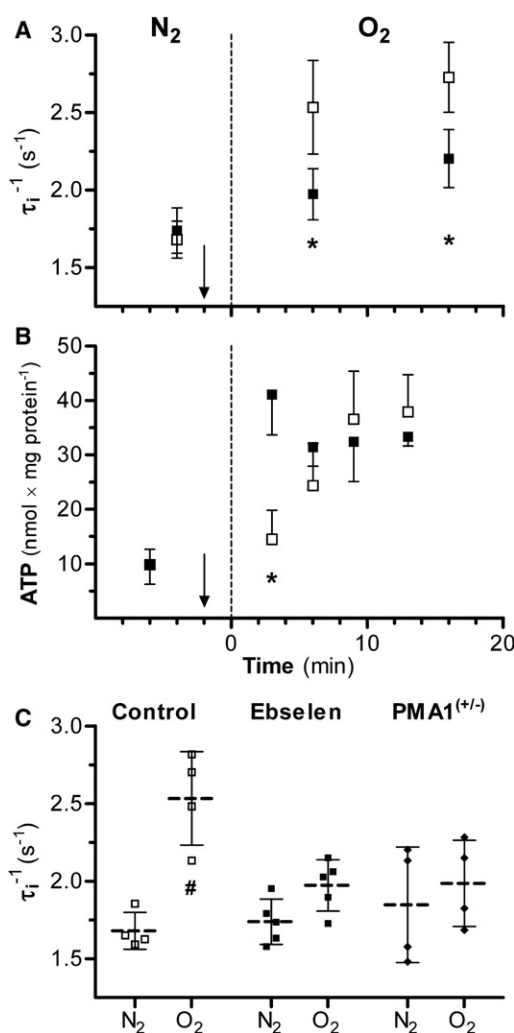


FIGURE 4 (A and B) Effect of increasing yeast plasma membrane H<sup>+</sup>-ATPase activity by switching from N<sub>2</sub> to O<sub>2</sub> (dashed line) at  $t = 0$ . (Arrows) At  $-2$  min, either DMSO alone (control) or a DMSO solution of ebselen (2-phenyl-1,2-benzisoxazol-3(2H), an H<sup>+</sup>-ATPase inhibitor) was added to the suspension. Mean ( $\pm$  SD); (asterisk)  $p < 0.05$  ebselen versus control. (A)  $\tau_i^{-1}$  for control ( $\square$ ,  $n = 4$ ) and ebselen-treated ( $\blacksquare$ ,  $n = 5$ ) suspensions. (B) HPLC ATP measurements plotted from separate studies of control ( $\square$ ,  $n = 4$ ) and ebselen-treated ( $\blacksquare$ ,  $n = 4$ ) suspensions. (C)  $\tau_i^{-1}$  for ( $\square$ ) control, ( $\blacksquare$ ) ebselen-treated, and ( $\blacklozenge$ ) PMA1<sup>+/-</sup> yeast suspensions in the N<sub>2</sub> (4 min before O<sub>2</sub>) and O<sub>2</sub> conditions (6 min after N<sub>2</sub>).  $\tau_i^{-1}$  for control yeast suspensions increased going from N<sub>2</sub> to O<sub>2</sub> ( $p < 0.001$ ), whereas the ebselen-treated and PMA1<sup>+/-</sup> yeast  $\tau_i^{-1}$  values were unchanged. Control and ebselen-treated  $\tau_i^{-1}$  are from panel A. The individual measurement values as well as the mean (dashed) and SD (solid) horizontal lines are shown. (Pound sign)  $p < 0.05$  O<sub>2</sub> versus N<sub>2</sub> same group.

if  $p < 0.05$ . GraphPad Prism (5.0 for Windows, GraphPad Software, San Diego, CA) was used for plots.

## RESULTS

### Relaxographic data and analyses

The quantity  $[(M_0(\infty) - M_z(t_I))/2M_0(\infty)]$  is calculated from the IR measurement data and 2SX fitting analyzes the data

(points) with the Bloch equations modified for two-site-exchange, Eqs. 4–7 (Fig. 1, upper panel). The solid curve results from the 2SX fitting with the variables returned:  $\tau_i = 0.54$  s,  $p_i = 0.11$ , and  $r_{1e} = 4.07$  s<sup>-1</sup> mM<sup>-1</sup>. As is seen, the quality of the fitting is quite high. Except at very small  $t_I$  values (likely due to imperfect inversion and/or magnetization transfer from yeast macromolecular <sup>1</sup>H resonances), the fitting residuals (lower panel) are essentially zero.

### Oxygenation dependence of water exchange kinetics

$R_{1L}$  was found to depend on oxygenation state, e.g., Fig. S1 and Fig. S3 in the Supporting Material. To explore this observation,  $\tau_i^{-1}$  (s<sup>-1</sup>), which equals  $k_{ie}$  (19), was determined under aerobic and anaerobic conditions (Fig. 2 A). During O<sub>2</sub> bubbling at 25°C,  $\tau_i^{-1}$  was constant at 3.1 ( $\pm 0.08$ ) s<sup>-1</sup>; after changing to N<sub>2</sub>,  $\tau_i^{-1}$  decreased exponentially until, after 95 min, it reached 1.5 ( $\pm 0.09$ ) s<sup>-1</sup>, an ~50% decrease.

The H<sub>2</sub>O<sub>i</sub> mole fraction,  $p_i$ , was 0.074 ( $\pm 0.005$ ) during the aerobic period; after the switch to N<sub>2</sub>,  $p_i$  increased by 23%, to 0.092 ( $\pm 0.006$ ) ( $p < 0.05$ ) (Fig. 2 B). The  $p_i$  change was essentially complete by 15 min, i.e., at the first post-switch measurement. This is much faster, and smaller, percentage-wise, than the  $\tau_i^{-1}$  change.

The quantity  $\tau_i^{-1}$  can be expressed as  $P_w(A/V)$ , where  $P_w$  is the water permeability coefficient, and  $V$  and  $A$  are the individual cell volume and surface area values, respectively (5). The N<sub>2</sub>-induced  $\tau_i^{-1}$  decrease (Fig. 2 A) may thus reflect decreases in  $P_w$ , ( $A/V$ ), or both. To examine this, we modeled the yeast cell as a sphere, so  $\tau_i^{-1} = 3P_w/r$  (radius  $r$ ). After switching to N<sub>2</sub>,  $3/r$  decreases by only ~7% (assumes  $V \propto p_i$ ). This suggests the N<sub>2</sub>-induced 50%  $\tau_i^{-1}$  reduction is dominated by a  $P_w$  decrease.

### Oxygenation dependence of ATP level

With no exogenous glucose, changing suspension oxygenation alters cellular energetics (20). <sup>31</sup>P MR measured yeast ATP content decreases rapidly after the switch to N<sub>2</sub> (Fig. 3 A), correlating with the  $\tau_i^{-1}$  decrease (Fig. 2 A). Although <sup>31</sup>P MR measurements are dynamic, rigorous quantifications are difficult because polyphosphate and ATP signals overlap (20). Thus, ATP content was also measured by HPLC. Three yeast strains, D273-10B, BY, and MR6  $\rho+$  (lacks the *ade2* gene), were used. Because MR6  $\rho+$  yeast requires adenine in the growth medium for purine biosynthesis, adjusting its concentration allows experimental control of steady-state aerobic ATP content. A strong correlation between  $\tau_i^{-1}$  and HPLC-measured ATP is observed (Fig. 3 B), which encompasses three yeast strains, both aerobic and anaerobic. The  $\tau_i^{-1}$  value increases at least linearly with ATP content, over almost two orders of magnitude.

## Involvement of the plasma membrane H<sup>+</sup>-ATPase

The  $\tau_i^{-1}$  ATP correlation suggests that equilibrium trans-plasma membrane water kinetics have contributions from active processes in addition to passive diffusion. The active yeast plasma membrane ion transport protein is a P-type H<sup>+</sup>-ATPase, which uses ATP hydrolysis energy to pump H<sup>+</sup> out of the cell. This creates an electrochemical proton gradient that establishes the membrane potential and drives much of the other transport via H<sup>+</sup>-dependent cotransporters. To test a H<sup>+</sup>-ATPase activity link to equilibrium water exchange, anaerobic suspensions were treated with ebselen, a cell membrane H<sup>+</sup>-ATPase inhibitor (11), and then energized with O<sub>2</sub>. The control suspension  $\tau_i^{-1}$  (Fig. 4 A) increased from 1.7 ( $\pm 0.1$ ) s<sup>-1</sup> to 2.5 ( $\pm 0.3$ ) s<sup>-1</sup> 6 min after the O<sub>2</sub> switch ( $p < 0.001$ ). In contrast, the ebselen-treated yeast  $\tau_i^{-1}$  was only 2.0 ( $\pm 0.2$ ) s<sup>-1</sup> at 6 min ( $p = 0.65$ ), and its  $\tau_i^{-1}$  value at 16 min was still less than the control yeast. Thus, ebselen suppressed the O<sub>2</sub>-induced  $\tau_i^{-1}$  increase. The  $p_i$  value initially decreased during O<sub>2</sub> in ebselen-treated and control cells (see Fig. S5 A). By 16 min, however, the ebselen-treated  $p_i$  had returned to its anaerobic value, whereas the control  $p_i$  remained small. Because  $V/A$  follows as the cube root of  $p_i$  (see above), we conclude that O<sub>2</sub> induces a  $P_w$  increase in control but not ebselen-treated yeast. Ebselen does not inhibit ATP synthesis. Three min after the O<sub>2</sub> switch, the ATP content of the ebselen-treated yeast exceeded that of the control yeast (Fig. 4 B). By the first  $\tau_i^{-1}$  measurement (6 min), however, the ATP contents of the control and ebselen-treated yeast were equal. Thus, the reduced water exchange kinetics in ebselen-treated yeast does not result from reduced ATP. This is consistent with  $\tau_i^{-1}$  being associated with H<sup>+</sup>-ATPase activity.

PMA1<sup>(+/-)</sup> diploid yeasts underwent the same protocol, without ebselen. These cells are deficient in one copy of the PMA1 gene, which encodes the P-type H<sup>+</sup>-ATPase. The O<sub>2</sub>  $\tau_i^{-1}$  responses of PMA1<sup>(+/-)</sup> and ebselen-treated yeast suspensions are remarkably similar (Fig. 4 C). This lends support to the notion that H<sup>+</sup>-ATPase activity is responsible for a significant portion of the  $\tau_i^{-1}$  and  $P_w$  increase with yeast cell energization.

## DISCUSSION

Water is usually in thermodynamic equilibrium (steady state) across the cell plasma membrane: i.e., the extra- and intracellular water chemical potentials are equal. Although our method measures steady-state trans-plasma membrane water exchange, it also detects net cellular water fluxes. A water influx causing an ~20% yeast cell volume increase occurs after switching from O<sub>2</sub> to N<sub>2</sub> (Fig. 2 B). This must reflect a net influx of solutes (ions) and/or production of intracellular metabolic osmolytes; most probably an intracellular osmolarity increase associated with anaerobic

metabolism. It represents a regulatory volume increase and is complete within 15 min of the gas change. The pseudo-first-order rate constant for this net influx equals 0.012 min<sup>-1</sup> ( $2.0 \times 10^{-4}$  s<sup>-1</sup>). This net water flux is described by the hydraulic permeability coefficient,  $P_f$ , to distinguish it from the equilibrium coefficient ( $P_d$ , termed  $P_w$  here) for which there is no net flux. Simultaneously, <sup>1</sup>H<sub>2</sub>O T<sub>1</sub> MRR/RR<sub>e</sub> 2SX analysis, and other NMR methods (21), measure diffusional water exchange kinetics, i.e., for equilibrium (steady state, reversible) trans-plasma membrane water molecule interchange. The rate constant equals  $k_{ie} + k_{ei}$  and when ATP > 50 nmol/mg protein (Fig. 3 B), it equals 3.2 s<sup>-1</sup>, four orders-of-magnitude larger than net influx rate constant. This rapid water exchange persists before, during, and after any net water flux.

The results demonstrate that  $\tau_i^{-1}$  correlates (at least linearly) with cellular ATP content. The ATP = 0 intercept of the Fig. 3 B line is  $\tau_i^{-1} = 1.2$  s<sup>-1</sup>. Using 2.3  $\mu$ m as anaerobic  $r$  (see Materials and Methods), the expression  $P_w = r/(3\tau_i)$  yields  $P_w = 9.2 \times 10^{-5}$  cm/s. This value is bracketed by the  $P_d$  values of  $8.1 \times 10^{-5}$  and  $57.3 \times 10^{-5}$  cm/s for sphingomyelin/cholesterol and phosphatidylcholine/cholesterol bilayer membranes, respectively, at the same temperature, 25°C (22). These values are for model bilayer membranes containing no proteins. This indicates that, in the absence of ATP and an osmotic gradient, water crosses the yeast cell membrane by simple, passive, unfacilitated diffusion directly across the plasma membrane lipid bilayer. The ATP = 0 intercept corresponds to a  $\tau_i$  value of 830 ms, which agrees with the  $\tau_i$  values of 700 ms (21) and 670 ms (5) reported in previous NMR studies of Bakers yeasts at similar temperatures and likely almost as ATP depleted. The method employed by Tanner (21) was different from that of Labadie (5).

One can use the rate constant  $\tau_i^{-1}$  ( $k_{ie}$ ), 1.2 s<sup>-1</sup>, (Fig. 3 B), for simple, passive, unfacilitated diffusion across the plasma membrane lipid bilayer to calculate the steady-state efflux of water molecules from the yeast cells at near minimum velocity. Thus, an anaerobic cell volume of 52.1 fL and an [H<sub>2</sub>O] of 50 mol/L yields  $1.57 \times 10^{12}$  molecules/cell; multiplying by 1.2 s<sup>-1</sup> yields an efflux of  $1.9 \times 10^{12}$  water molecules/s/cell. Likewise, using the aerobic condition rate constant  $\tau_i^{-1}$  ( $k_{ie}$ ), ~3 s<sup>-1</sup> (Figs. 2 A and 3 B), with an aerobic cell volume of 42.2 fL, yields an efflux of  $3.8 \times 10^{12}$  water molecules/s/cell. For both conditions there must be equal numbers of water molecules entering the cell per second. Thus, the velocity of yeast water efflux (and influx) increases by a factor of 2 (~ $1.9 \times 10^{12}$  water molecules/s/cell) going from passive, unfacilitated diffusion across the plasma membrane lipid bilayer to the active component, with cellular ATP  $\cong$  70 nmol/mg protein, during oxidative metabolism.

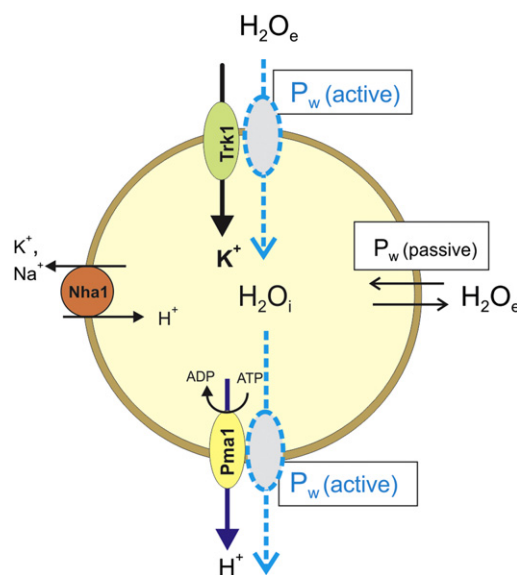
With cellular ATP >35 nmol/mg protein, yeast trans-plasma membrane equilibrium water exchange has an active component (a good reason to use  $P_w$  instead

of  $P_d$ ):  $P_w = P_w(\text{passive}) + P_w(\text{active})$ . The most obvious way for ATP to influence water exchange is for water to accompany active trans-plasma membrane transport, ion pumping, and/or secondary cotransport. Our finding that reducing  $H^+$ -ATPase activity with an inhibitor or genetic modification of  $H^+$ -ATPase expression reduces  $\tau_i^{-1}$ , even with adequate ATP, supports this idea. We are not aware that an active water cycling consequent to transport activity has been previously described.

The P-type  $H^+$ -ATPase utilizes the Gibbs free energy of ATP hydrolysis,  $\Delta G_{ATP}$  to transport  $H^+$  out of the cell in an osmogenic, electrogenic reaction. This generates the electrochemical  $H^+$  gradient (23) that is the primary energy source for secondary transport in the yeast. The observed increase in  $\tau_i^{-1}$  ( $\sim P_w$ ) associated with  $H^+$ -ATPase activity (Fig. 4) could result from water cotransport with its primary process ( $H_i^+ \rightarrow H_e^+$ ) and/or with secondary transport processes, such as of other ions (e.g.,  $Na^+$  and  $K^+$ ), driven by the  $H^+$  electrochemical gradient. This is suggested in the Fig. 5 cartoon, which indicates selected proteins: the  $H^+$ -ATPase (Pma1), the  $H^+/K^+, Na^+$  antiporter (Nha1), and the  $K^+$  transporter (Trk1) (24). It is possible that any, or all, of these proteins (as well as others) enable transmembrane water movement (25). The dashed membrane-spanning ovals in Fig. 5 suggest water cotransported or facilitated water diffusion with the activities of these proteins. Together, they constitute an active, equilibrium transmembrane water cycling consequent to homeostatic ion or metabolite transport processes.

Water cotransport describes the secondary active transport of water (25). The sodium-dependent glucose cotransporter, SGLT1 (26), has been reported to conduct secondary active water cotransport (27). The energy for this was obtained from that released by the substrate flux. Others have contested water cotransport by SGLT1, finding that water transport was passive and required the osmotic gradient created by sodium and glucose transport (28). SGLT1-expressing oocytes displayed a twofold increase in passive water permeability that was sensitive to the specific inhibitor phlorizin (28). The protein acted as a conduit for the water driven by the osmotic gradient. We denote the protein-mediated increase in water permeability resulting from local osmotic gradients as facilitated water diffusion.

Although it is reasonable that the Fig. 5 dashed ovals represent water cotransported (or experiencing facilitated diffusion) with the ions or molecules transported by membrane transporter enzymes, cellular volume does not vary. Consequently, the entire cellular ensemble of membrane water transporter proteins would have to work in concert transporting water in opposite directions in a perfectly balanced manner. We know that the cell does this for the ions. Alternatively, it is possible that the dashed ovals in Fig. 5 represent an enhanced exchange of intra- and extracellular water that occurs during protein transport activity. Because this mechanism involves water exchange



Web 3C

FIGURE 5 Cartoon depicting transmembrane water cycling in a yeast cell. Several plasma membrane ion transporters with hypothetical water cotransport or facilitated diffusion (dashed ovals) are shown. The major ion transport protein is the electrogenic P-type  $H^+$ -ATPase (Pma1), which pumps  $H^+$  out of the cell at the expense of ATP. Also shown are the  $K^+$  uniporter (Trk1) and the  $H^+/K^+, Na^+$  antiporter (Nha1). Water-facilitated diffusion or cotransport could be through one or both of the following: 1), water cavities in the ion transporter molecules or 2), the ion channels themselves. Integrated over the entire cell, this represents active transmembrane water cycling accompanying the ion transport of the membrane transport enzymes. The active components,  $P_w(\text{active})$ , associated with protein activity, and passive components,  $P_w(\text{passive})$ , associated with the membrane, of the total membrane water permeability ( $P_w$ ) are also indicated. Because cellular volume does not vary, at least on the macroscopic timescale, the membrane water cotransport or facilitated diffusion mechanisms requires that the entire cellular ensemble of water transporters must function in a balanced manner. Alternatively, it is possible that the dashed ovals represent intra- and extracellular water exchanging (i.e., the dashed oval arrows would be bidirectional) during protein transport activity. Because this mechanism involves water exchange and not transport, volume is unaffected.

and not cotransport or facilitated diffusion, volume is unaffected.

Water can also move through aquaporins, membrane water channel proteins. Aquaporin-1 increases net water permeation 10- to 100-fold, in response to an osmotic gradient (29). Although aquaporin-1 can catalyze passive water exchange, as in the erythrocyte, it does not itself facilitate active water exchange (25). In most laboratory *S. cerevisiae* strains, the aquaporin-encoding genes (AQY1 and AQY2) contain inactivating mutations (30) and, thus, aquaporins are not normally active as water channels. For the phenomenon we observe, the Fig. 5 dashed ovals almost certainly are not aquaporins.

Pma1 contains a central aqueous cavity that is connected via columns of water molecules, which function as proton ( $H^+$ ) wires, to the inlet and outlet sides of the protein (31). It is possible that Pma1 activity increases fusion of

the central-water-filled cavity with the inlet and outlets, thus increasing transmembrane H<sub>2</sub>O cotransport or exchange. Lactose permease (LacY), a lactose proton symporter, and other major facilitator superfamily proteins, include an interior aqueous cavity (32). This cavity contains the H<sup>+</sup> and lactose binding sites; is large enough to hold >400 water molecules; and, is alternately accessible to the intra- and extracellular environments during transport activity, favoring transmembrane H<sub>2</sub>O exchange or facilitated diffusion. Because LacY uses the electrochemical H<sup>+</sup> gradient to transport lactose, amplified water exchange, i.e., active water cycling, during activity could be a general characteristic of many transporters. Aqueous cavities exist in a number of membrane channels and pumps (33).

The H<sup>+</sup>-ATPase of plants and fungi and the related P-type ATPase (the Na<sup>+</sup>/K<sup>+</sup> ATPase) of animal cells each create the primary ion gradient used as an energy source for secondary transport. It is possible that water also cycles across the mammalian plasma membrane in concert with Na<sup>+</sup> ion pumping and exchange.

### Possible implications of active water cycling for <sup>1</sup>H MRI

Mean human tissue  $\tau_i$  values have been estimated in vivo from minimally invasive Dynamic-Contrast-Enhanced-MRI data (6,19), where the contrast reagent acts as an RR<sub>c</sub>. The  $\tau_i$  parameter is averaged over a region-of-interest or, if signal/noise permits, an image voxel. Parametric  $\tau_i$  maps of a human MS lesion (34), an osteosarcoma (34), and malignant breast (34,35) tumors have been reported. Note that  $\tau_i$  is proportional to a one-dimensional measure of individual cell size (and inversely proportional to  $P_w$ ), and not the intravoxel cell volume fraction. It is an intensive property, independent of the number of cells in the voxel (cellularity). This is elaborated in Strijkers et al. (15). Tissues accessible to RR<sub>c</sub> (heart, liver, kidney, skeletal muscle) provide pathologies amenable to investigation. It is tempting to speculate that  $\tau_i^{-1}$  may provide a means to differentiate pathologies, based on their transmembrane water exchange kinetics as a measure of metabolic activity (membrane exchange activity) and/or cell volume changes.

The brain parenchyma is not normally RR accessible due to the relative impermeability of the brain blood barrier. However, the mean capillary (blood) water lifetime,  $\tau_b$ , can be determined in DCE-MRI studies, and mapped, and varies in MS pathology (36). Thus,  $\tau_b^{-1} = (P_w)_{\text{capillary}}(2/r)_{\text{capillary}}$ , where  $(P_w)_{\text{capillary}}$  is the water permeability coefficient for the vessel wall, which is comprised chiefly of endothelial cells. Their plasma membranes are surely engaged in homeostatic ion cycling.

Our finding of an active component of  $\tau_i^{-1}(P_w)$  may have implications for understanding the changes in diffusion-weighted MRI seen after stroke (37). The early decrease (30%) in the cerebral tissue water apparent water diffusion

coefficient (ADC) was ascribed to a net water influx (or cell swelling) mechanism and large differences between intra- and extracellular water ADC values (38). It is now known that these ADC values are not sufficiently different and a metabolically related intracellular water ( $ADC_i$ ) decrease appears more plausible (39). A model of water diffusion in axons predicts a compartmental membrane permeation rate-limiting step (40). It is possible that diffusion of intracellular water in normally energized cells includes water cycling across organelle (mitochondria, endoplasmic reticula, etc.) as well as plasma membranes. As O<sub>2</sub> deprivation in stroke causes rapid ATP depletion, active ion pumping will quickly cease. A concomitant transmembrane water cycling decrease could be reflected as an  $ADC_i$  decrease. Alternatively, organelle swelling could occur upon deoxygenation. From the principles elucidated here,  $1/\tau_{\text{organelle}} \propto (P_w)_{\text{organelle}}(A/V)_{\text{organelle}}$ . Possibly both effects occur, each factor decreases, and a  $\tau_{\text{organelle}}$  increase causes an  $ADC_i$  decrease.

### CONCLUSIONS

Water actively cycles across the yeast plasma membrane consequent to membrane protein transport activity. Active water cycling during such activity may be a general characteristic of cells. It is an interesting question as to why non-aquaporin protein water transport capacity exists. Erythrocytes contain abundant aquaporin and display very rapid water exchange. Kuchel and Benga (41) proposed two hypotheses to explain natural selection for high erythrocyte water permeability via aquaporin: 1), the membrane has energy-dependent undulations and the energy expended is minimized by avoiding water displacement; and 2), the rapid facilitated diffusion of glucose, chloride, and bicarbonate across the membrane would cause volume change if water was not displaced. Erythrocyte water exchange is, however, reduced only ~50% by aquaporin inhibition (4). Facilitated diffusion of water by membrane transport proteins may provide an explanation for some of the substantial nonaquaporin erythrocyte water permeability.

Noting that aquaporin is not crucial for whole body water homeostasis, Zeuthen (25) claims that much transepithelial water transport occurs through other proteins by the cotransport and/or facilitated diffusion mechanisms. Active water cycling may be a mechanism that enables cells to minimize (or avoid) transmembrane osmotic pressure gradients resulting from metabolic transport activity. With its rapid kinetics the active transmembrane water cycle has the capacity to handle rapid changes in intra- or extracellular osmotic pressure, i.e., the small-scale local osmotic gradients that are inherent in many transport and/or metabolic processes. This mechanism would keep the transmembrane osmotic pressure gradient at a minimum (or zero) and maintain steady-state cellular volume, which is important for cellular homeostasis. The proteins that mediate the water cycle may

also be a component of the system that transports water in response to large-scale osmotic pressure differences.

## SUPPORTING MATERIAL

Methods and Materials and Results sections, as well as five figures and three tables, are available at [http://www.biophysj.org/biophysj/supplemental/S0006-3495\(11\)01257-4](http://www.biophysj.org/biophysj/supplemental/S0006-3495(11)01257-4).

We thank Prof. Jean-Paul di Rago, Universite Victor Segalen, for providing the MR6  $\rho+$  yeast.

National Institutes of Health grants HL078634 (J.A.B.), EB-00422, and NS-40801 (C.S.S.), supported this work.

## REFERENCES

1. Verkman, A. S. 2000. Water permeability measurement in living cells and complex tissues. *J. Membr. Biol.* 173:73–87.
2. House, C. R. 1974. Water Transport in Cells and Tissues. E. Arnold, London.
3. Conlon, T., and R. Outhred. 1972. Water diffusion permeability of erythrocytes using an NMR technique. *Biochim. Biophys. Acta.* 288:354–361.
4. Benga, G., B. E. Chapman, and P. W. Kuchel. 2009. Comparative NMR studies of diffusional water permeability of red blood cells from different species: XV. Agile wallaby (*Macropus agilis*), red-necked wallaby (*Macropus rufogriseus*) and Goodfellow's tree kangaroo (*Dendrolagus goodfellowi*). *Comp. Biochem. Physiol. A Mol. Integr. Physiol.* 154:105–109.
5. Labadie, C., J. H. Lee, ..., C. S. Springer, Jr. 1994. Relaxographic imaging. *J. Magn. Reson. B.* 105:99–112.
6. Li, X., W. Huang, ..., C. S. Springer, Jr. 2008. Dynamic NMR effects in breast cancer dynamic-contrast-enhanced MRI. *Proc. Natl. Acad. Sci. USA.* 105:17937–17942.
7. Zhang, Y., M. Poirer-Quinot, ..., J. A. Balschi. 2010. Discrimination of intra- and extracellular  $^{23}\text{Na}^+$  signals in yeast cell suspensions using longitudinal magnetic resonance relaxography. *J. Magn. Reson.* 205:28–37.
8. Landis, C. S., X. Li, ..., C. S. Springer, Jr. 1999. Equilibrium transcytlemmal water-exchange kinetics in skeletal muscle in vivo. *Magn. Reson. Med.* 42:467–478.
9. Poirer-Quinot, M., H. He, ..., J. A. Balschi. 2006.  $^1\text{H}_2\text{O}$  relaxography of the perfused rat heart. In ISMRM 14th Scientific Meeting.. Wiley Interscience, Seattle, WA. 1176.
10. Vagabov, V. M., L. V. Trilisenko, and I. S. Kulaev. 2000. Dependence of inorganic polyphosphate chain length on the orthophosphate content in the culture medium of the yeast *Saccharomyces cerevisiae*. *Biochemistry (Mosc.)*. 65:349–354.
11. Chan, G., D. Hardej, ..., B. Billack. 2007. Evaluation of the antimicrobial activity of ebselen: role of the yeast plasma membrane  $\text{H}^+$ -ATPase. *J. Biochem. Mol. Toxicol.* 21:252–264.
12. Rak, M., E. Tetaud, ..., J. P. di Rago. 2007. Yeast cells lacking the mitochondrial gene encoding the ATP synthase subunit 6 exhibit a selective loss of complex IV and unusual mitochondrial morphology. *J. Biol. Chem.* 282:10853–10864.
13. Chu, S. C., M. M. Pike, ..., C. S. Springer, Jr. 1984. Aqueous shift reagents for high-resolution cationic nuclear magnetic resonance. III.  $\text{Dy}(\text{TTHA})^{3-}$ ,  $\text{Tm}(\text{TTHA})^{3-}$ , and  $\text{Tm}(\text{PPP})_2^{7-}$ . *J. Magn. Reson.* 56:33–47.
14. Bretthorst, G. L., J. J. Kotyk, and J. J. Ackerman. 1989.  $^{31}\text{P}$  NMR Bayesian spectral analysis of rat brain in vivo. *Magn. Reson. Med.* 9:282–287.
15. Strijkers, G. J., S. Hak, ..., K. Nicolay. 2009. Three-compartment  $T_1$  relaxation model for intracellular paramagnetic contrast agents. *Magn. Reson. Med.* 61:1049–1058.
16. Yankeelov, T. E., W. D. Rooney, ..., C. S. Springer, Jr. 2003. Variation of the relaxographic “shutter-speed” for transcytlemmal water exchange affects the CR bolus-tracking curve shape. *Magn. Reson. Med.* 50:1151–1169.
17. Jorgensen, P., J. L. Nishikawa, ..., M. Tyers. 2002. Systematic identification of pathways that couple cell growth and division in yeast. *Science.* 297:395–400.
18. Lowry, O. H., N. J. Rosebrough, ..., R. J. Randall. 1951. Protein measurement with the Folin phenol reagent. *J. Biol. Chem.* 193:265–275.
19. Huang, W., X. Li, ..., C. S. Springer. 2008. The magnetic resonance shutter speed discriminates vascular properties of malignant and benign breast tumors in vivo. *Proc. Natl. Acad. Sci. USA.* 105:17943–17948.
20. Höfeler, H., D. Jensen, ..., J. A. Balschi. 1987. Sodium transport and phosphorus metabolism in sodium-loaded yeast: simultaneous observation with sodium-23 and phosphorus-31 NMR spectroscopy in vivo. *Biochemistry.* 26:4953–4962.
21. Tanner, J. E. 1983. Intracellular diffusion of water. *Arch. Biochem. Biophys.* 224:416–428.
22. Finkelstein, A. 1987. Water Movement Through Lipid Bilayers, Pores, and Plasma Membranes: Theory and Reality. John Wiley & Sons, New York.
23. Ambesi, A., M. Miranda, ..., C. W. Slayman. 2000. Biogenesis and function of the yeast plasma-membrane  $\text{H}^+$ -ATPase. *J. Exp. Biol.* 203:155–160.
24. Ariño, J., J. Ramos, and H. Sychrová. 2010. Alkali metal cation transport and homeostasis in yeasts. *Microbiol. Mol. Biol. Rev.* 74:95–120.
25. Zeuthen, T. 2010. Water-transporting proteins. *J. Membr. Biol.* 234:57–73.
26. Loo, D. D., B. A. Hirayama, ..., E. M. Wright. 1999. Passive water and ion transport by cotransporters. *J. Physiol.* 518:195–202.
27. Zeuthen, T., A. K. Meinild, ..., T. Litman. 1997. Water transport by the  $\text{Na}^+$ /glucose cotransporter under isotonic conditions. *Biol. Cell.* 89:307–312.
28. Duquette, P. P., P. Bissonnette, and J. Y. Lapointe. 2001. Local osmotic gradients drive the water flux associated with  $\text{Na}^+$ /glucose cotransport. *Proc. Natl. Acad. Sci. USA.* 98:3796–3801.
29. Agre, P., L. S. King, ..., S. Nielsen. 2002. Aquaporin water channels—from atomic structure to clinical medicine. *J. Physiol.* 542:3–16.
30. Meyrial, V., V. Laizé, ..., F. Tacnet. 2001. Existence of a tightly regulated water channel in *Saccharomyces cerevisiae*. *Eur. J. Biochem.* 268:334–343.
31. Buch-Pedersen, M. J., B. P. Pedersen, ..., M. G. Palmgren. 2009. Protons and how they are transported by proton pumps. *Pflugers Arch.* 457:573–579.
32. Abramson, J., S. Iwata, and H. R. Kaback. 2004. Lactose permease as a paradigm for membrane transport proteins (Review). *Mol. Membr. Biol.* 21:227–236 (Review).
33. Gouaux, E., and R. Mackinnon. 2005. Principles of selective ion transport in channels and pumps. *Science.* 310:1461–1465.
34. Yankeelov, T. E., W. D. Rooney, ..., C. S. Springer, Jr. 2005. Evidence for shutter-speed variation in CR bolus-tracking studies of human pathology. *NMR Biomed.* 18:173–185.
35. Li, X., W. Huang, ..., C. S. Springer, Jr. 2005. Shutter-speed analysis of contrast reagent bolus-tracking data: preliminary observations in benign and malignant breast disease. *Magn. Reson. Med.* 53:724–729.
36. Rooney, W.D., X. Li, ..., C.S. Springer. 2004. First pass bolus-tracking measurement of transendothelial water exchange in healthy controls. In International Society of Magnetic Resonance in Medicine, 12th Annual Meeting. 1390.

37. Moseley, M. E., Y. Cohen, ..., P. R. Weinstein. 1990. Early detection of regional cerebral ischemia in cats: comparison of diffusion- and T2-weighted MRI and spectroscopy. *Magn. Reson. Med.* 14:330–346.
38. Benveniste, H., L. W. Hedlund, and G. A. Johnson. 1992. Mechanism of detection of acute cerebral ischemia in rats by diffusion-weighted magnetic resonance microscopy. *Stroke.* 23:746–754.
39. Ackerman, J. J., and J. J. Neil. 2010. The use of MR-detectable reporter molecules and ions to evaluate diffusion in normal and ischemic brain. *NMR Biomed.* 23:725–733.
40. Fieremans, E., D. S. Novikov, ..., J. A. Helpert. 2010. Monte Carlo study of a two-compartment exchange model of diffusion. *NMR Biomed.* 23:711–724.
41. Kuchel, P. W., and G. Benga. 2005. Why does the mammalian red blood cell have aquaporins? *Biosystems.* 82:189–196.